

# Journal of Biomedical Optics

[SPIEDigitalLibrary.org/jbo](http://SPIEDigitalLibrary.org/jbo)

## **Lipid droplet pattern and nondroplet-like structure in two *fat* mutants of *Caenorhabditis elegans* revealed by coherent anti-Stokes Raman scattering microscopy**

Yung-Hsiang Yi  
Cheng-Hao Chien  
Wei-Wen Chen  
Tian-Hsiang Ma  
Kuan-Yu Liu  
Yu-Sun Chang  
Ta-Chau Chang  
Szecheng J. Lo

# Lipid droplet pattern and nondroplet-like structure in two *fat* mutants of *Caenorhabditis elegans* revealed by coherent anti-Stokes Raman scattering microscopy

Yung-Hsiang Yi,<sup>a\*</sup> Cheng-Hao Chien,<sup>c,d\*</sup> Wei-Wen Chen,<sup>c,e,f</sup> Tian-Hsiang Ma,<sup>a</sup> Kuan-Yu Liu,<sup>b</sup> Yu-Sun Chang,<sup>a</sup> Ta-Chau Chang,<sup>c,d</sup> and Szecheng J. Lo<sup>a,b</sup>

<sup>a</sup>Chang Gung University, Center of Molecular Medicine, College of Medicine, Kwei-Shan, Tao-Yuan 333, Taiwan

<sup>b</sup>Chang Gung University, Department of Biomedical Sciences, College of Medicine, Kwei-Shan, Tao-Yuan 333, Taiwan

<sup>c</sup>Academia Sinica, Institute of Atomic and Molecular Sciences, Taipei 106, Taiwan

<sup>d</sup>National Yang-Ming University, Institute of Biophotonics, Taipei 112, Taiwan

<sup>e</sup>Academia Sinica, Institute of Atomic and Molecular Sciences, Molecular Science and Technology Program,

Taiwan International Graduate Program, Taipei 106, Taiwan

<sup>f</sup>National Tsing Hua University, Department of Chemistry, Hsinchu 300, Taiwan

**Abstract.** Lipid is an important energy source and essential component for plasma and organelle membranes in all kinds of cells. Coherent anti-Stokes Raman scattering (CARS) microscopy is a label-free and nonlinear optical technique that can be used to monitor the lipid distribution in live organisms. Here, we utilize CARS microscopy to investigate the pattern of lipid droplets in two live *Caenorhabditis elegans* mutants (*fat-2* and *fat-3*). The CARS images showed a striking decrease in the size, number, and content of lipid droplets in the *fat-2* mutant but a slight difference in the *fat-3* mutant as compared with the wild-type worm. Moreover, a nondroplet-like structure with enhanced CARS signal was detected for the first time in the uterus of *fat-2* and *fat-3* mutants. In addition, transgenic *fat-2* mutant expressing a GFP fusion protein of vitellogenin-2 (a yolk lipoprotein) revealed that the enhanced CARS signal colocalized with the GFP signal, which suggests that the nondroplet-like structure is primarily due to the accumulation of yolk lipoproteins. Together, this study implies that CARS microscopy is a potential tool to study the distribution of yolk lipoproteins, in addition to lipid droplets, in live animals. © 2014 Society of Photo-Optical Instrumentation Engineers (SPIE) [DOI: 10.1117/1.JBO.19.1.011011]

Keywords: coherent anti-Stokes Raman scattering microscopy; *Caenorhabditis elegans*; lipid droplet; lipid metabolism; *fat-2*; *fat-3*; yolk lipoprotein; vitellogenin-2.

Paper 130304SSRR received May 1, 2013; revised manuscript received Jul. 18, 2013; accepted for publication Jul. 22, 2013; published online Aug. 26, 2013.

## 1 Introduction

Lipids are varied in form and function in living organisms. One of the well-known functions is to serve as a major energy source, which is stored in the lipid droplet organelle.<sup>1,2</sup> Morphologically, they appear in a globular shape but vary in size, ranging from submicron to tens of microns in most cells. Lipid droplets are composed of a hydrophobic core containing neutral lipids, mainly triglyceride (TG) and cholesteryl esters, which is surrounded by a monolayer of phospholipids with structural proteins of perilipin.<sup>3</sup> Lipid metabolism is evolutionarily conserved from bacteria to humans<sup>4</sup> and plays important roles in energy homeostasis, which is critical for the regulation in cell survival, growth, reproduction, and aging.<sup>5</sup> Many human diseases, such as diabetes, atherosclerosis, and the metabolic syndrome, are found to be associated with lipid droplet accumulation.<sup>6</sup> However, the detailed mechanism remains largely unrevealed.

*Caenorhabditis elegans* (*C. elegans*) is a well-established animal model to study lipid metabolism because of the following advantages: a short life cycle, easy handling, cost saving, convenient for genetic approaches, easy to obtain mutants, and available in whole genome (RNA interference) clones for knockdown of specific genes to study its gene functions.<sup>7-9</sup> Genes involved in desaturation of lipid biosynthesis pathway are well characterized in *C. elegans*, including *fat-1* to *fat-7* genes. In this pathway, only *fat-2* (delta-12 fatty acid desaturase) is involved in the desaturation of C18 monounsaturated fatty acid to C18 polyunsaturated fatty acid (PUFA). On the other hand, three *fat* genes—*fat-1* (omega-3 fatty acid desaturase), *fat-3* (delta-6 fatty acid desaturase), and *fat-4* (delta-5 fatty acid desaturase)—are involved in the biosynthesis of C20 PUFA.<sup>10</sup> Accordingly, among all *fat* genes, *fat-2* plays a unique and pivotal role in the biosynthesis of PUFA, which is the major component in TG and can be stored in lipid droplets.<sup>9,10</sup> In previous studies, RNAi knockdown of *fat-2* gene showed a notable decrease in body fat of *C. elegans* and a dramatic phenotype in low brood size and hatching rate,<sup>10,11</sup> while the *fat-3* mutant had reduction of C20 PUFA and a decrease in brood size.<sup>12</sup>

Recently, coherent Raman scattering (CRS) techniques, such as coherent anti-Stokes Raman scattering (CARS) and stimulated Raman scattering (SRS) microscopies, have been applied

\*Yung-Hsiang Yi and Cheng-Hao Chien have equal contribution.

Address all correspondence to: Ta-Chau Chang, Academia Sinica, Institute of Atomic and Molecular Sciences, Taipei 106, Taiwan. Tel: 886-2-2366-8231; Fax: 886-2-23620200; E-mail: tcchang@po.iams.sinica.edu.tw; Szecheng J. Lo, Chang Gung University, Department of Biomedical Sciences, TaoYuan 333, Taiwan. Tel: +886-3-2118800 ext 3295; Fax: +886-3-2118392; E-mail: losj@mail.cgu.edu.tw

to *in vivo* imaging of lipid droplet distribution in *C. elegans*.<sup>13–18</sup> Their advantages include label-free, three-dimensional sectioning, and specificity to lipid, which make them powerful imaging tools for characterization and quantification of lipid in live animals.<sup>17,18</sup> For example, Hellerer et al. observed more lipid droplets in the hypodermis of the *daf-2* and *daf-4* dauer mutants than of the wild type.<sup>13</sup> Yen et al. performed a comparative study of fat storage quantification in *C. elegans* using label and label-free methods.<sup>14</sup> They found that both vital dye and fixative staining methods may lead to wrong interpretation of lipid storage, while CARS microscopy provides more reliable quantification results.<sup>14</sup> Le et al. reported label-free visualization of neutral and autofluorescent lipid droplets by using CARS coupled with two-photon excited fluorescence (TPEF) microscopy, and used the expression level between neutral and autofluorescent lipid droplets to assay the genotype–phenotype relationship of mutants in *C. elegans*.<sup>15</sup> Moreover, Wang et al. discovered several new lipid-regulating genes by RNAi screening based on SRS microscopy.<sup>16</sup> These reports revealed the capability and potentiality of CRS microscopy to the research of lipid biology in *C. elegans*.

Many of the mutants with impaired lipid metabolism in *C. elegans* have been examined by dye-staining methods (e.g., Nile Red); however, their lipid droplet patterns have not been well characterized in detail. In this work, we utilized CARS microscopy to investigate and characterize lipid droplet patterns of *fat-2* and *fat-3* mutants by quantitative analysis. Compared with Nile Red staining, the CARS microscopy showed even better sensitivity, specificity, and resolution for lipid imaging, as well as for lipid droplet quantification. We measured the size, number, and content of lipid droplets in the wild type, *fat-2*, and *fat-3* mutants. In addition, we report the first observation of nondroplet-like structure in the uterus of *fat-2* and *fat-3* mutants by using CARS microscopy. Moreover, the nondroplet-like structure was contributed by the accumulation of yolk lipoproteins, as revealed by fluorescence and CARS microscopy.

## 2 Materials and Methods

### 2.1 Worm Strains and Reagents

Wild type (Bristol N2), CB1370 [*daf-2* (*e1370*)], BX26 [*fat-2* (*wa17*)], and BX30 [*fat-3* (*wa22*)] mutant *C. elegans* were obtained from the Caenorhabditis Genetics Center. The *fat-2* (*wa17*); *vit-2p::vit-2::gfp* mutant was a gift from Dr. M. A. Miller (University of Alabama, Birmingham, Alabama). Nile Red was purchased from Invitrogen (Grand Island, New York) for detection of lipid droplets. Levamisole was purchased from Sigma (St. Louis, Missouri) and used to paralyze worms for microscopy.

### 2.2 Maintenance of *C. elegans*

All strains used in this study were cultured on nematode growth medium plate seeded with an *E. coli* OP50 and incubated at 20 to 22°C.<sup>19</sup> Animals were analyzed by using Nile Red staining and CARS/TPEF microscopy.

### 2.3 Nile Red Staining and Colocalization Analysis

Approximately 500 to 1000 larva 4 stage *C. elegans* were collected and washed twice by using phosphate-buffered saline (PBS) buffer. For fixation, worms were transferred to modified Ruvkun's Witches Brew solution (80 mM KCl, 20 mM NaCl,

7 mM ethylene glycol tetraacetic acid, 15 mM 1,4-Piperazinediethanesulfonic acid pH 7.4, 0.5 mM spermidine, 1% formaldehyde, 0.1% mercaptoethanol) in liquid nitrogen to freeze and thawed for 1 h.<sup>20</sup> Fixation solution was removed by washing twice in PBS buffer and worms were transferred to 1 ml M9 buffer with or without Nile Red dye (1  $\mu$ g/ml) and incubated at 4°C for 30 min. After washing twice with PBS to remove staining solution, worms were mounted on 5% agar pad for microscopy. The colocalization between CARS and Nile Red staining images was analyzed by using MetaMorph software (version 7.5, Molecular Devices, California).<sup>21</sup> Both CARS and Nile Red images were thresholded to mark the area of lipid droplets. Colocalization of CARS over Nile Red is defined as the overlapping area of CARS over Nile Red, divided by the area of CARS (%). The colocalization between CARS and VIT-2::GFP fluorescence images was analyzed by the same protocol as described above.

### 2.4 CARS/TPEF Microscopy and Lipid Droplet Quantification

Nile Red stained worms were collected as described above. For live worm imaging, ~40 worms were collected and paralyzed on

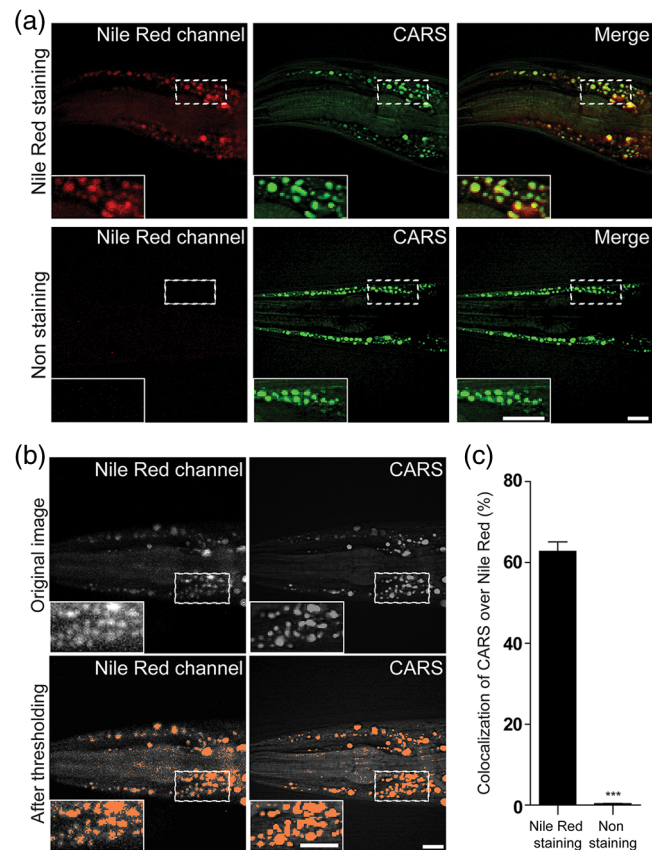


**Fig. 1** The comparison of Nile Red and CARS imaging in detecting lipid droplets of *C. elegans*. (a) Nile Red fluorescence and CARS images of lipid droplets in fixed worms with (upper row) or without (lower row) Nile Red staining (the heads of wild-type worms at larva 4 stage). Their merged images are shown in the right column. (b) Nile Red fluorescence and CARS images before (upper row) and after (lower row) thresholding. (c) The colocalization of CARS over Nile Red image. Data are from three independent experiments. Scale bars represent 10  $\mu$ m. The numbers (*n*) of worms for each condition are as follows: for Nile Red staining, *n* = 35; for non-Nile Red staining, *n* = 30. Error bars indicate standard error of mean (SEM). \*\*\**P* < 0.001.

the agar pad. Lipid droplets and Nile Red or GFP fluorescence were monitored using CARS and TPEF microscopy, respectively. The setup of CARS was described in the previous report.<sup>22</sup> Briefly, two Ti-sapphire laser beams (Mira-900P and Mira-900F, Coherent, California) were synchronized by Synchro-Lock system (Coherent, California) and tuned at  $\sim 710$  and  $\sim 890$  nm to obtain CARS imaging of lipid C-H stretching mode at  $\sim 2845$   $\text{cm}^{-1}$ . The forward CARS signal (at  $\sim 590$  nm) is collected by a condenser (NA = 0.55), passing through a set of bandpass filters (FF01-630/92 and FF01-590/10, Semrock, New York) and detected by a photomultiplier tube (PMT) (R7400U-02, Hamamatsu, Japan). Fluorescence signal was collected by a  $60\times$  NA = 1.2 water immersion objective, passing through a bandpass filter (FF01-624/40 for Nile Red and FF01-512/25 for GFP, Semrock, Rochester, New York), and detected by a PMT (R3896, Hamamatsu, Japan). The background, defined as the average intensity of CARS, was subtracted from the original image for quantification of CARS intensity.<sup>15</sup> The number, size, and CARS intensity of lipid droplets were analyzed by using the MetaMorph software version 7.5.

### 3 Results and Discussion

#### 3.1 Detecting Lipid Droplets in *C. elegans* by Nile Red Fluorescence and CARS Microscopy

The distribution of lipid droplets in worms can be revealed by Nile Red staining, a common fluorescence indicator of neutral lipids. To evaluate the capability of CARS imaging on lipids of *C. elegans*, we compared the CARS and Nile Red fluorescence images of larva 4 stage worms with or without Nile Red staining. Lipid droplets in the hypodermis cell were easily detected by both methods [Fig. 1(a), upper row]. While almost no signal was detected in worms without Nile Red staining by TPEF microscopy, lipid droplets were clearly detected in the same worm by CARS microscopy [Fig. 1(a), lower row]. The colocalization of the lipid droplets between Nile Red fluorescence and CARS images is shown in Fig. 1(a) (right column). To estimate this colocalization, both CARS and Nile Red staining images were thresholded to mark the area of lipid droplets [Fig. 1(b), lower row], followed by the calculation of the colocalization (see Materials and Methods for the detailed description). The result shows a high colocalization of CARS over Nile Red

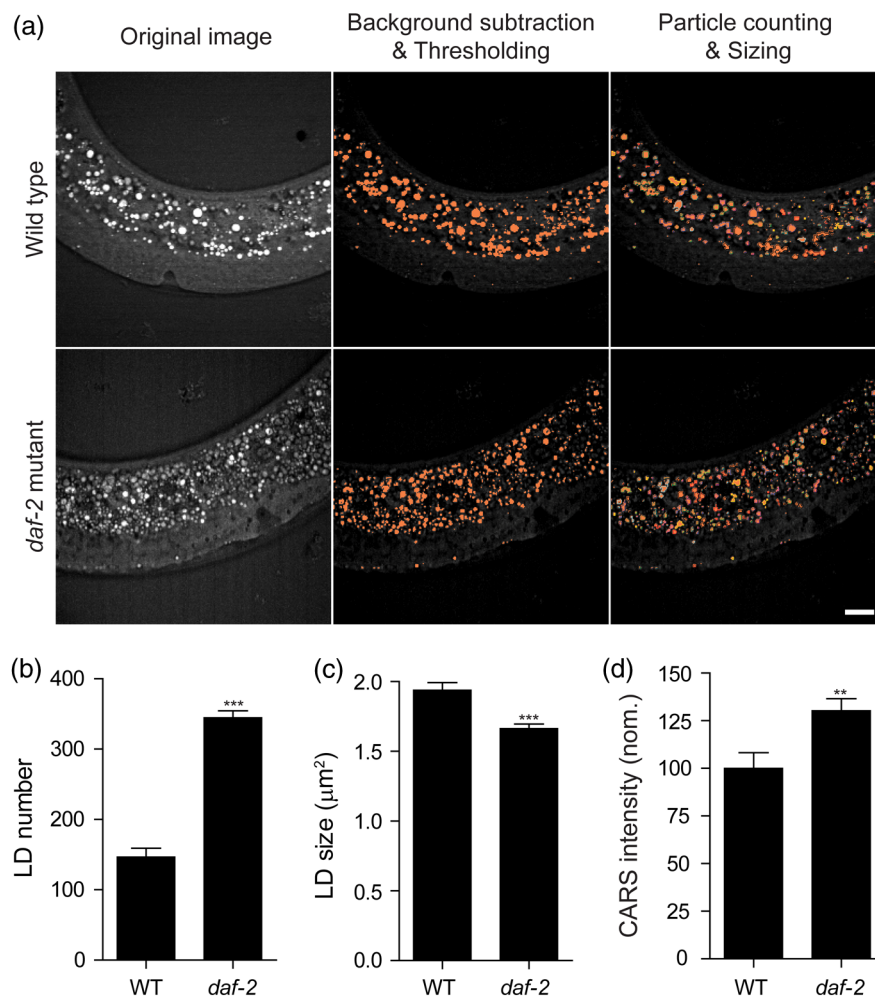


**Fig. 2** Lipid droplets in the wild type (WT) and *daf-2* mutant. (a) The analysis process of CARS images for lipid droplet quantification in the larva 4 stage of the WT and *daf-2* mutant. The scale bar represents 10  $\mu\text{m}$ . Quantification of the number (b), size (c), and CARS intensity (d) of their lipid droplets. Data are from three independent experiments. The numbers (*n*) of worms for each strain are as follows: WT, *n* = 20; *daf-2*, *n* = 20. Error bars indicate SEM. \*\**P* < 0.01; \*\*\**P* < 0.001.

( $62.7 \pm 2.3\%$ ) of worms with Nile Red staining, while almost no colocalization ( $0.4 \pm 0.1\%$ ) is present in the sample without Nile Red staining [Fig. 1(c)]. These data indicate that the CARS signal well colocalizes with Nile Red signal in stained *C. elegans*. Furthermore, the enlarged images [the insets of Figs. 1(a) and 1(b)] clearly show that the resolution and contrast of the CARS image are better than those of the Nile Red fluorescence image, suggesting that CARS microscopy is a better method to visualize small lipid droplets.<sup>18</sup> In contrast to the Nile Red staining method that requires sample fixation, CARS microscopy can be used to visualize lipid droplets directly in live organisms without labeling. This enables CARS microscopy to monitor dynamic change of lipid droplet distribution.

The *daf-2* gene encodes for the insulin-like growth factor 1 receptor in *C. elegans* and is involved in the regulation of the life span.<sup>23</sup> The *daf-2* strain is known as a lipid-enriched mutant in *C. elegans* and has been studied by using CARS microscopy.<sup>13,14,24</sup> We next examined *daf-2* mutant to testify the quantification method of CARS images [Fig. 2(a)]. For quantification, after background subtraction and image thresholding, the lipid droplet regions were marked [Fig. 2(a) middle column], counted (number), and measured (size, intensity) by the software [Fig. 2(a) right column). Compared with previous reports,<sup>13,14,24</sup> similar quantitative results were obtained showing that the number and content of lipid droplets significantly increase in *daf-2* mutant [Figs. 2(b) and 2(d)]. In contrast, we found that the lipid droplet size decreases in *daf-2* mutant [Fig. 2(c)], while previous reports showed no statistical difference.<sup>13,14,24</sup> Different results of lipid droplet size may be due to the various stages of worms used. Nevertheless, the good specificity and sensitivity of CARS microscopy with label-free imaging, can provide a powerful tool to monitor and characterize lipid droplet distribution in live *C. elegans*.

### 3.2 Significant Decrease of Lipid Droplets in *Fat-2* Mutant

Although the body fat of *fat-2* and *fat-3* mutants has been examined by Nile Red staining and gas chromatography,<sup>11,12</sup> their lipid droplet patterns have not been characterized in detail. Here we used CARS microscopy to visualize their lipid in live worms and analyzed their lipid droplets. Figure 3(a) shows CARS images of the wild type, *fat-2*, and *fat-3* mutants. Our results show a drastic decrease of lipid droplet number in *fat-2* but not in *fat-3* mutant [Fig. 3(b)]. Remarkable decreases in lipid droplet size and content were also found in the *fat-2* mutant worms, while only a slight increase in lipid droplet size and a decrease in lipid content were observed in the *fat-3* mutant [Figs. 3(c) and 3(d)]. Taken together, these data indicate that the loss of *fat-2* function, but not *fat-3*, causes a significant decrease in number, size, and content of lipid droplets in *C. elegans*. In previous studies, *fat-2* was well documented to be the upstream of *fat-3* and is the unique enzyme to participate in the first step of PUFA biosynthesis.<sup>10</sup> Consistently, we found more phenotypic changes of lipid droplets in *fat-2* than in *fat-3* mutant. To our knowledge, this is the first detailed characterization of lipid droplet patterns in *fat-2* and *fat-3* mutants. Our results suggest that the downregulation of PUFA synthesis in *fat-2* mutant can be directly revealed by the change of lipid droplet pattern.

### 3.3 NonDroplet-Like Structure with Enhanced CARS Signal in the Uterus of *Fat-2* and *Fat-3* Mutants

In addition to lipid droplet structure, an enhanced CARS signal located in the uterus of *fat-2* and *fat-3* mutants was detected in contrast to little or no signal in the uterus of the wild type [arrowheads in Fig. 4(a)]. A higher percentage of worms in

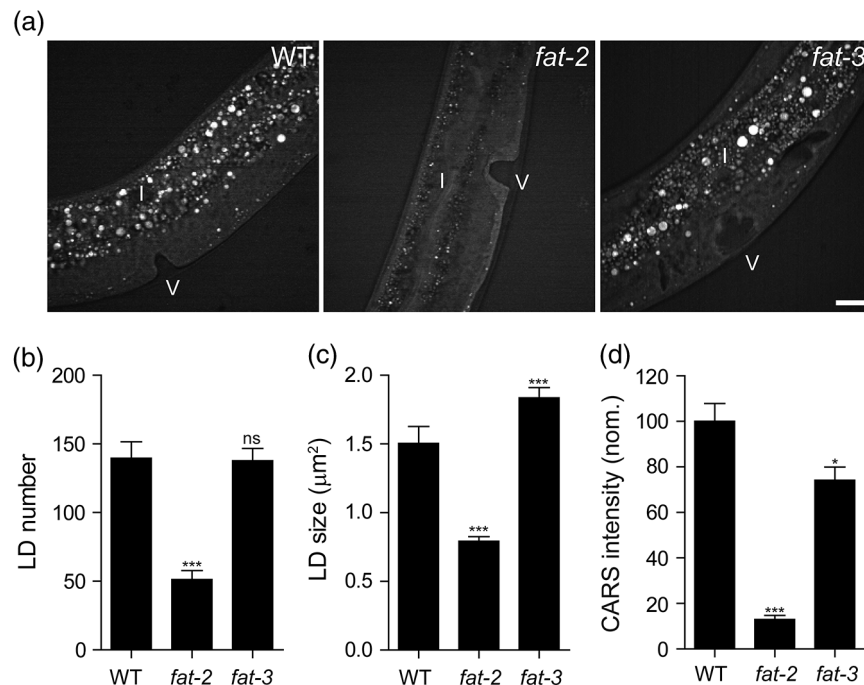


**Fig. 3** Lipid droplets in the WT, *fat-2*, and *fat-3* mutants. (a) CARS images of the larva 4 stage worms in the WT, *fat-2*, and *fat-3* mutants. The scale bar represents 10  $\mu\text{m}$ . I, intestine; V, vulva. Quantification of the number (b), size (c), and CARS intensity (d) of their lipid droplets. Data are from three independent experiments. The numbers (*n*) of worms for each strain are as follows: WT, *n* = 25; *fat-2*, *n* = 16; *fat-3*, *n* = 20. Error bars indicate SEM. \* $P < 0.05$ ; \*\*\* $P < 0.001$ ; ns, no significance.

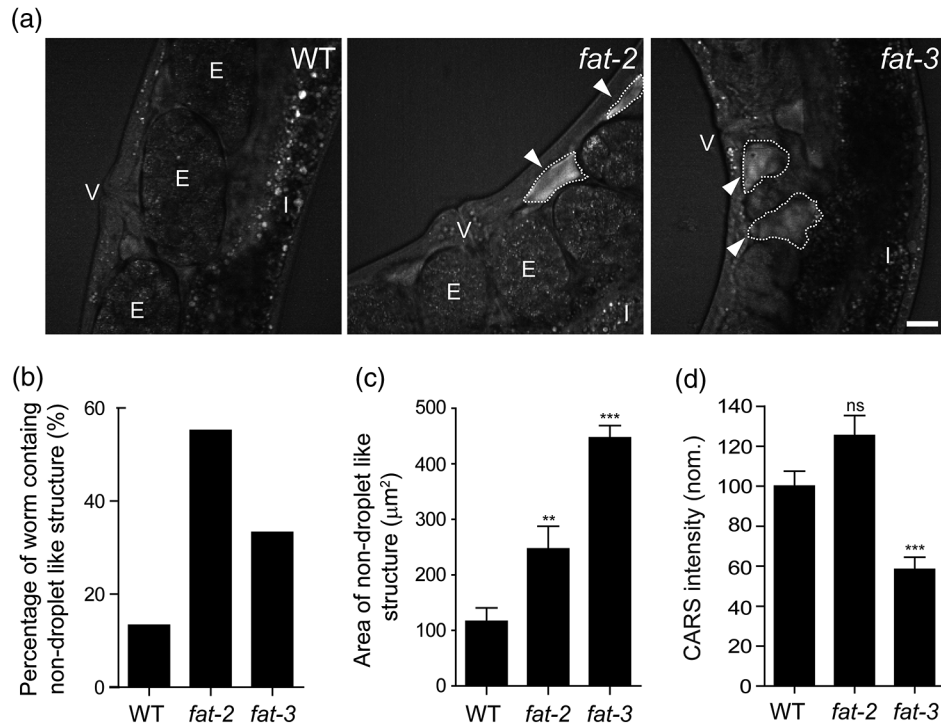


**Fig. 4** The nondroplet-like structure with enhanced CARS signal in the uterus of *C. elegans* at the adult stage. (a) CARS images show the uterus of WT, *fat-2*, and *fat-3* mutants. Arrowheads and dashed lines indicate the nondroplet-like structure. The scale bar represents 10  $\mu\text{m}$ . E, embryo; I, intestine; V, vulva. (b) Percentage of worms containing nondroplet-like structure in the uterus as indicated. Data are from three independent experiments. The numbers (*n*) of worms for each strain are as follows: WT, *n* = 89; *fat-2*, *n* = 29; *fat-3*, *n* = 36. (c) The quantified area (c) and averaged intensity (d) of the nondroplet-like structure in different strains as indicated. The numbers (*n*) of worms for each strain are as follows: WT, *n* = 14; *fat-2*, *n* = 16; *fat-3*, *n* = 12. Error bars indicate SEM. \*\**P* < 0.01; \*\*\**P* < 0.001; ns, no significance.

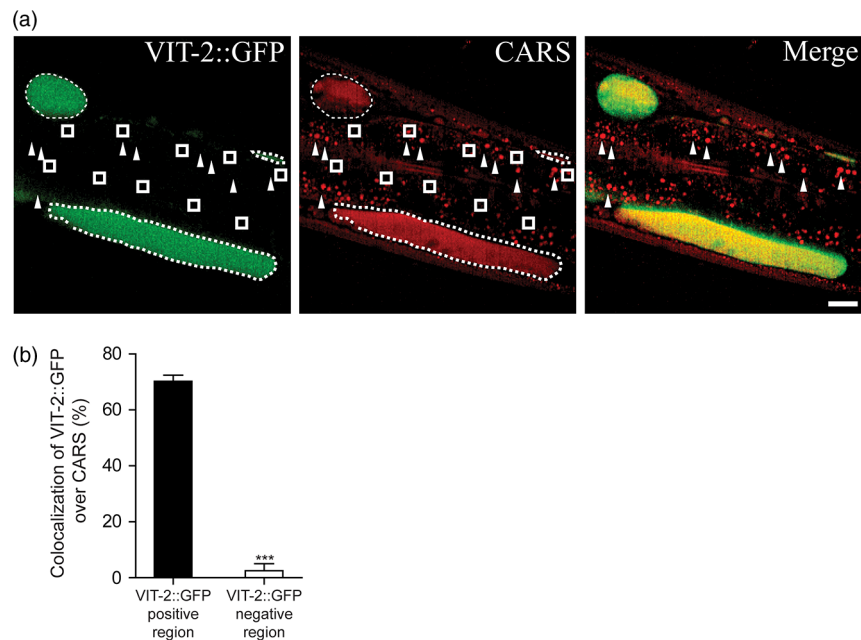


**Fig. 5** The colocalization between VIT-2::GFP fluorescence and CARS signal of the nondroplet-like structure in the uterus of *fat-2* mutant at the adult stage. (a) VIT-2::GFP fluorescence image (left column), CARS image (middle column), and their merged image (right column) of the uterus in live *fat-2* mutant. VIT-2::GFP positive regions are labeled by dash line, and VIT-2::GFP negative regions are randomly selected and labeled in squares. Lipid droplets in CARS image are indicated by arrowheads. Scale bar represents 10  $\mu\text{m}$ . (b) The colocalization of VIT-2::GFP fluorescence over CARS signal in VIT-2::GFP positive and negative regions. The number of worms is 13. Error bars indicate SEM. \*\*\**P* < 0.001.

the *fat-2* mutant contains such nondroplet-like structure in the uterus than that of the *fat-3* mutant [55.2% versus 33.3%, Fig. 4(b)]. Additionally, an increase of nondroplet-like structure area was found in both *fat-2* and *fat-3* mutants as compared with the wild type [Fig. 4(c)]. However, the CARS intensities of nondroplet-like structure in the wild type and *fat-2* mutant are stronger than in the *fat-3* mutant [Fig. 4(d)]. This nondroplet-like structure with enhanced CARS signal in both *fat-2* and *fat-3* mutants was not reported before. In previous studies, *fat-2* mutation is well known to cause a reduction in the level of PUFA,<sup>9</sup> which is required for lipid transportation from intestine to oocytes by yolk lipoproteins.<sup>25</sup> Edmonds et al. found an obvious accumulation of yolk lipoprotein in the uterus of the *fat-2* mutant by using vitellogenin-2::GFP fusion protein as an indicator.<sup>26</sup> This suggests that the nondroplet-like structure with enhanced CARS signal in the uterus of the *fat-2* mutant may come from the accumulation of yolk lipoproteins.

To test the hypothesis, we compared the pattern of CARS signal of nondroplet-like structure with the fluorescence signal of yolk lipoprotein reporter (vitellogenin-2::GFP) in the uterus of the *fat-2* mutant. The yolk lipoprotein reporter was detected by TPEF microscopy [dashed line in Fig. 5(a)] as well as by CARS microscopy. In contrast, lipid droplets [arrowheads in Fig. 5(a)] were only detectable in CARS but not in a fluorescence channel. In colocalization analysis, Fig. 5(b) demonstrates high colocalization of CARS over VIT-2::GFP ( $70.2 \pm 2.2\%$ ) in the VIT-2::GFP positive regions of the *fat-2* mutant [dash line in Fig. 5(a)], whereas there is almost no colocalization ( $2.5 \pm 2.5\%$ ) in the VIT-2::GFP negative regions [randomly selected and shown in squares in Fig. 5(a)]. Yolk lipoproteins are well characterized as lipid transporters from intestine to gonad and provide the essential nutrients for embryo development.<sup>27</sup> They are composed of lipid-binding proteins (vitellogenin-1 to 6) and lipid<sup>28</sup> that can be detected by CARS microscopy. In previous studies, *fat-2* mutation causes the disorder in biosynthesis of PUFA,<sup>9</sup> which is required for endocytosis of yolk lipoproteins (by using exogenous vitellogenin-2::GFP reporter) into oocytes via the low-density lipoprotein receptor (RME-2, receptor-mediated endocytosis-2).<sup>25,27</sup> In this study, we demonstrate that PUFA biosynthesis is required for endocytosis of “native” yolk lipoproteins in live animals without labeling, and the first visualize of the accumulation of native yolk lipoproteins in the uterus of the *fat-2* mutant is shown by using CARS microscopy. It remains unclear whether the accumulation of yolk lipoproteins is a common phenotype in other mutants impaired in lipid metabolism.

#### 4 Conclusion

In this study, we used Nile Red staining and CARS microscopy to investigate lipid droplet distribution in *C. elegans*. Compared with Nile Red staining, CARS microscopy has better specificity as well as sensitivity for lipid droplet imaging and is more applicable for observation of lipid droplet distribution in live organisms. We further studied two *fat* mutants, *fat-2* and *fat-3*, and found a notable decrease in lipid droplet number, size, and content in the *fat-2* mutant, while only a slight increase in lipid droplet size and a decrease in lipid content of the *fat-3* mutant were found. In addition, we observed nondroplet-like structure with enhanced CARS signal in the uterus of *fat-2* and *fat-3* mutants, which has not been reported before. The enhanced CARS signal of nondroplet-like structure is contributed from the accumulation of yolk lipoproteins, resulting from the loss

of PUFA in mutants with metabolic defects in fatty acid biosynthesis. Our work demonstrates that CARS microscopy can provide more detailed information of lipid and yolk lipoprotein distribution in live *C. elegans* without labeling. This imaging tool can be further used to monitor the dynamic change of lipid and yolk lipoprotein distribution and study their formation, disruption, and translocation in live animals during development. By using CARS microscopy, we found a new phenotype of native yolk lipoprotein accumulation in the uterus, which correlates with the defect in yolk lipoprotein transportation. This experimental platform is applicable to the screen of other gene candidates that are involved in the regulation of yolk lipoprotein transportation.

#### Acknowledgments

We thank Dr. M. A. Miller (University of Alabama, Birmingham, Alabama) for providing us *fat-2(wa17); vit-2p::vit-2::gfp* mutant *C. elegans*, and Caenorhabditis Genetics Center for other mutant strains. We are grateful to Dr. Margaret Hsin-Jui Kuo (Academia Sinica) for her valuable discussion and careful reading of the manuscript. We also thank the microscope core facility of Molecular Medicine Research Center at Chang Gung University for providing the services. This work was supported by the grant of Ministry of Education, the National Science Council of the Republic of China (Grant Nos. NSC100-2511-S-182-001 and NSC101-2113-M-001-022), and Chang-Gung Memorial Hospital (Grant No. EMRPD1B0081).

#### References

1. E. Bieberich, “It’s a lipid’s world: bioactive lipid metabolism and signaling in neural stem cell differentiation,” *Neurochem. Res.* **37**(6), 1208–1229 (2012).
2. S. D. Gilk, “Role of lipids in *Coxiella burnetii* infection,” *Adv. Exp. Med. Biol.* **984**, 199–213 (2012).
3. M. Digel, R. Eehalt, and J. Fullekrug, “Lipid droplets lighting up: insights from live microscopy,” *FEBS Lett.* **584**(11), 2168–2175 (2010).
4. P. S. Aguilar and D. de Mendoza, “Control of fatty acid desaturation: a mechanism conserved from bacteria to humans,” *Mol. Microbiol.* **62**(6), 1507–1514 (2006).
5. M. Hansen, T. Flatt, and H. Aguilaniu, “Reproduction, fat metabolism, and life span: what is the connection?,” *Cell Metab.* **17**(1), 10–19 (2013).
6. K. Reue and E. Board, “A thematic review series: lipid droplet storage and metabolism: from yeast to man,” *J. Lipid Res.* **52**(11), 1865–1868 (2011).
7. C. Wilkins et al., “RNA interference is an antiviral defence mechanism in *Caenorhabditis elegans*,” *Nature* **436**(7053), 1044–1047 (2005).
8. R. S. Kamath and J. Ahringer, “Genome-wide RNAi screening in *Caenorhabditis elegans*,” *Methods* **30**(4), 313–321 (2003).
9. J. L. Watts, “Fat synthesis and adiposity regulation in *Caenorhabditis elegans*,” *Trends Endocrinol. Metab.* **20**(2), 58–65 (2009).
10. J. L. Watts and J. Browse, “Genetic dissection of polyunsaturated fatty acid synthesis in *Caenorhabditis elegans*,” *Proc. Natl. Acad. Sci. USA* **99**(9), 5854–5859 (2002).
11. M. Horikawa et al., “Elongation and desaturation of fatty acids are critical in growth, lipid metabolism and ontogeny of *Caenorhabditis elegans*,” *J. Biochem.* **144**(2), 149–158 (2008).
12. J. L. Watts et al., “Deficiencies in C20 polyunsaturated fatty acids cause behavioral and developmental defects in *Caenorhabditis elegans fat-3* mutants,” *Genetics* **163**(2), 581–589 (2003).
13. T. Hellerer et al., “Monitoring of lipid storage in *Caenorhabditis elegans* using coherent anti-Stokes Raman scattering (CARS) microscopy,” *Proc. Natl. Acad. Sci. U.S.A.* **104**(37), 14658–14663 (2007).

14. K. Yen et al., "A comparative study of fat storage quantitation in nematode *Caenorhabditis elegans* using label and label-free methods," *PLoS ONE* **5**(9), e12810 (2010).
15. T. T. Le et al., "Label-free quantitative analysis of lipid metabolism in living *Caenorhabditis elegans*," *J. Lipid Res.* **51**(3), 672–677 (2010).
16. M. C. Wang et al., "RNAi screening for fat regulatory genes with SRS microscopy," *Nat. Methods* **8**(2), 135–138 (2011).
17. I. C. Elle et al., "Something worth dyeing for: molecular tools for the dissection of lipid metabolism in *Caenorhabditis elegans*," *FEBS Lett.* **584**(11), 2183–2193 (2010).
18. A. Follick, W. Min, and M. C. Wang, "Label-free imaging of lipid dynamics using coherent anti-stokes Raman scattering (CARS) and stimulated Raman scattering (SRS) microscopy," *Curr. Opin. Genet. Dev.* **21**(5), 585–590 (2011).
19. S. Brenner, "The genetics of *Caenorhabditis elegans*," *Genetics* **77**(1), 71–94 (1974).
20. K. K. Brooks, B. Liang, and J. L. Watts, "The influence of bacterial diet on fat storage in *C. elegans*," *PLoS ONE* **4**(10), e7545 (2009).
21. K. Hayakawa, H. Tatsumi, and M. Sokabe, "Actin filaments function as a tension sensor by tension-dependent binding of cofilin to the filament," *J. Cell Biol.* **195**(5), 721–727 (2011).
22. C. H. Chien et al., "Investigation of lipid homeostasis in living *Drosophila* by coherent anti-Stokes Raman scattering microscopy," *J. Biomed. Opt.* **17**(12), 126001 (2012).
23. S. Murakami, "Caenorhabditis elegans as a model system to study aging of learning and memory," *Mol. Neurobiol.* **35**(1), 85–94 (2007).
24. L. R. Lapiere et al., "Autophagy genes are required for normal lipid levels in *C. elegans*," *Autophagy* **9**(3), 278–286 (2013).
25. H. M. Kubagawa et al., "Oocyte signals derived from polyunsaturated fatty acids control sperm recruitment in vivo," *Nat. Cell. Biol.* **8**(10), 1143–1148 (2006).
26. J. W. Edmonds et al., "Insulin/FOXO signaling regulates ovarian prostaglandins critical for reproduction," *Dev. Cell* **19**(6), 858–871 (2010).
27. B. Grant and D. Hirsh, "Receptor-mediated endocytosis in the *Caenorhabditis elegans* oocyte," *Mol. Biol. Cell* **10**(12), 4311–4326 (1999).
28. W. J. Sharrock et al., "Two distinct yolk lipoprotein complexes from *Caenorhabditis elegans*," *J. Biol. Chem.* **265**(24), 14422–14431 (1990).